Novel Three-Phase PWM Voltage-Fed Rectifier with an Auxiliary Resonant Commutated Pole Link

Ke-Qing Qu[†] and Jin-Bin Zhao[*]

[†*]College of Electrical Engineering, Shanghai University of Electric Power, Shanghai, China

Abstract

A novel auxiliary resonant commutated pole (ARCP) link for three-phase PWM voltage-fed converter is presented. The ARCP link consists of two auxiliary switches, one resonant inductance, and six diodes, which is simpler than the conventional ARCP designs. Based on the phase and amplitude control, the proposed converter can take a minimum switching times PWM method, which results in reduced losses and a simplified control. In addition, the zero-voltage resonance modes are analyzed. Finally, simulation and experimental results show that the system can realize zero-voltage switching with a unity power factor.

Key words: ARCP, PFC, Zero voltage switching

I. INTRODUCTION

In order to obtain high power factor transmission of electric power and reduced switching loss simultaneously, soft-switching PWM converters have become an effective solution among modern power conversion devices for suppressing harmonic pollution, restraining electromagnetic interference and increasing efficiency.

There are a variety of topologies and control strategies for designing three phase soft switching PWM converters. Among these, the zero-voltage switching (ZVS) converters can be broadly divided into two categories according to the different bus links in achieving resonance: the resonant DC link system (RDCLS) [1]-[3] and the resonant pole system (RPS) [4]-[10]. The RDCLS uses a resonant circuit composing of resonant inductors paralleled on the DC bus and snubber capacitors paralleled on the power switches, which achieves a periodical zero voltage on the DC bus as a basis for the power switches turning-on. This solution is simple in structure. However, it affects utilization of the bus voltage. In comparison the RPS changes the resonant circuit being with resonant inductors paralleled in three-phase bridges on AC bus links, which scales the bridge input

voltage either at zero or at bus working voltage periodically, and so the power switches acts at zero voltage.

The auxiliary resonant commutated pole (ARCP) converters among the RPS solutions have some advantages, such as higher efficiency, lower voltage or current stress to the power switches and fly-wheel diodes. However, for the conventional ARCP three-phase PWM converter, each bridge with one resonant circuit has six auxiliary switches, three resonant inductors and six diodes, which lead to a complex structure. Some papers suggests a simplification of the structure of RPS converters so as to promoting their application [11]-[17].

A simplified ARCP for three-phase PWM rectifier is proposed in this paper, which includes two auxiliary switches, one resonant inductor and six diodes. Based on amplitude and phase control, the rectifier applies the least switching times PWM mode, which ensures a normal resonance to simplify the control, and improved efficiency. The six power switches in the three-phase bridges act under the ZVS state, while the two auxiliary switches work under the zero current switching (ZCS) state. The effectiveness of the proposed strategy is demonstrated through simulation and experiment results for a 1kW PWM rectifier.

II. MAIN CIRCUIT AND PWM CONTROL STRATEGY

Fig. 1 shows the main circuit of the proposed ARCP three-phase PWM rectifier, where e_R, e_S and e_T refer to
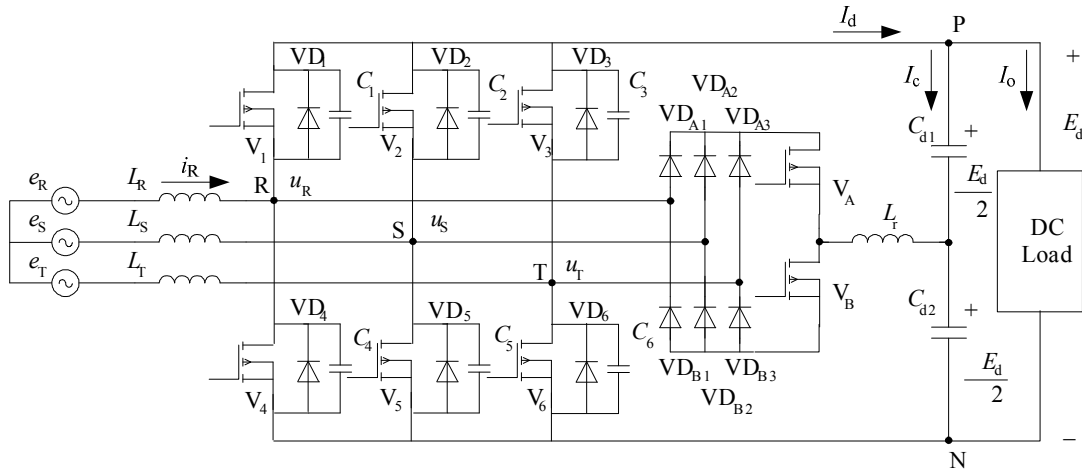
Fig. 1. Main circuit of the ARCP rectifier.

the three-phase AC source. The three-phase bridge circuit includes series inductances L_R, L_S and L_T, power switches V_1~V_6, fly-wheel diodes VD_1~VD_6, and snubber capacitors C_1~C_6. The resonance circuit is composed of diodes VD_{A1}~VD_{A3} and VD_{B1}~VD_{B3}, auxiliary switches V_A and V_B, split-capacitor capacitors C_{d1} and C_{d2}, and a resonant inductor L_r. The DC voltage on the load is defined as E_d and $E_d/2$ as the voltage on C_{d1} and C_{d2} respectively. The fundamental components of the phase voltage after PWM are u_R, u_S and u_T. The PWM control strategies of the rectifier are described in detail hereafter.

The rectifier applies amplitude and phase control to achieve power factor correction while the phase voltage and phase current are kept in phase. This complies with the following expressions:

$$\begin{cases} u_R(t) = M\sin(\omega t - \theta_0) \\ u_S(t) = M\sin(\omega t - \theta_0 - \dfrac{2\pi}{3}) \\ u_T(t) = M\sin(\omega t - \theta_0 - \dfrac{4\pi}{3}) \end{cases} \quad (1)$$

Where M is the modulation ratio, and θ_0 is the offset angle between u_R and e_R.

Fig. 2 shows the key waveforms, where i_R, i_S and i_T are the three-phase currents from the source, and u_R', u_S' and u_T' are the three-phase modulation waves. On the other hand, u_{G1}~u_{G6}, u_{GA} and u_{GB} are the gate drive signals of the power switches V_1~V_6, V_A and V_B. It can be seen from Fig.1 that each power switch in the three-phase bridges has one paralleled snubber capacitor that prevents immediate voltage changes. The switches always turn off in the ZVS state. Therefore, only turning-on of the power devices in the ZVS state is necessary. To conveniently achieve closing of the switches at the same time, in Fig.2 the modulation method adopts a saw-tooth carrier with alternative positive and negative slopes instead of the conventional triangular carrier. It is defined here that
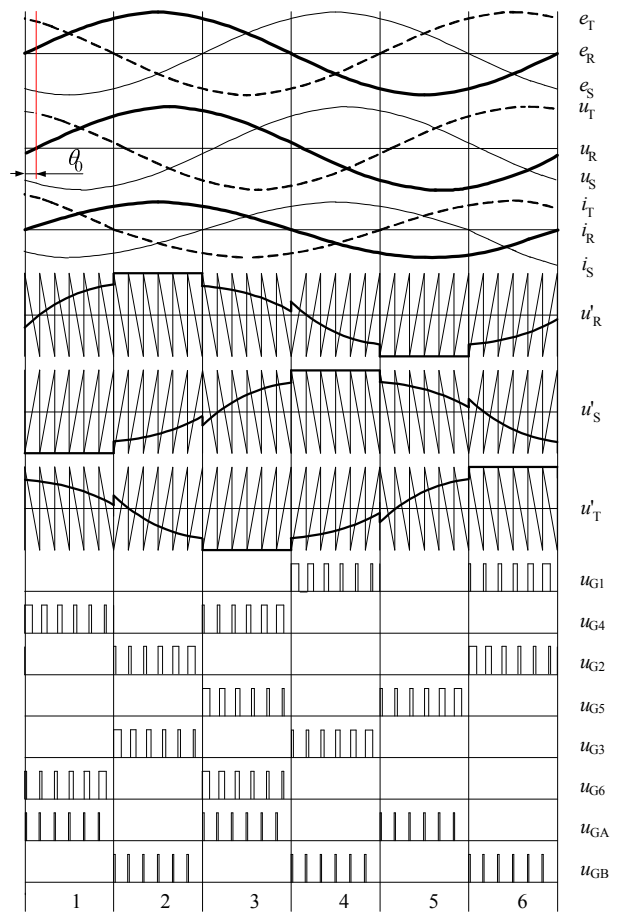

Fig. 2. Key waveforms of proposed converter.

when it flows to the power device, the phase current is positive and the saw-tooth carrier adopts a positive slope, or phase current is negative and the saw-tooth carrier adopts a negative slope. The turning-on of the power devices can be converged at the vertical edges of the saw-tooth carrier. When compared with the triangular carrier, the resonance control becomes easier and is reduces 1/3 resonant times.

The minimum switching time PWM mode is adopted to ensure auxiliary resonant converting. In Fig.2 the per cycle of [0, 2] can be divided into six sections according to the difference between a phase current direction to the other two phase currents. For instance in section 2, since the phase R current is at maximum, it flows though diode VD_1 in parallel with switch V_1. Then in the phase R bridge, the two power switches V_1 and V_4 are kept off. Therefore, the switching times can be cut down 1/3 when compared to the conventional methods. The control strategy achieves easier control of the system.

Three phase voltage modulation wave signals u_R', u_S' and u_T' are generated by the line voltage. According to the six sections mentioned above and by combining equation (1), the following expressions can be derived:

Section 1
$$\begin{cases} u_R'(t) = u_R(t) - u_S(t) - 1 = \sqrt{3}M\cos(\omega t - \theta_0 - \frac{\pi}{3}) - 1 \\ u_S'(t) = -1 \\ u_T'(t) = u_T(t) - u_S(t) - 1 = \sqrt{3}M\cos(\omega t - \theta_0) - 1 \end{cases}$$

Section 2
$$\begin{cases} u_R'(t) = +1 \\ u_S'(t) = u_S(t) - u_R(t) + 1 = -\sqrt{3}M\cos(\omega t - \theta_0 - \frac{\pi}{3}) + 1 \\ u_T'(t) = u_T(t) - u_R(t) + 1 = -\sqrt{3}M\cos(\omega t - \theta_0 - \frac{2\pi}{3}) + 1 \end{cases}$$

Section 3
$$\begin{cases} u_R'(t) = u_R(t) - u_T(t) - 1 = \sqrt{3}M\cos(\omega t - \theta_0 - \frac{2\pi}{3}) - 1 \\ u_S'(t) = u_S(t) - u_T(t) - 1 = \sqrt{3}M\cos(\omega t - \theta_0) - 1 \\ u_T'(t) = -1 \end{cases}$$

Section 4
$$\begin{cases} u_R'(t) = u_R(t) - u_S(t) + 1 = \sqrt{3}M\cos(\omega t - \theta_0 - \frac{\pi}{3}) + 1 \\ u_S'(t) = +1 \\ u_T'(t) = u_T(t) - u_S(t) + 1 = \sqrt{3}M\cos(\omega t - \theta_0) + 1 \end{cases}$$

Section 5
$$\begin{cases} u_R'(t) = -1 \\ u_S'(t) = u_S(t) - u_R(t) - 1 = -\sqrt{3}M\cos(\omega t - \theta_0 - \frac{\pi}{3}) - 1 \\ u_T'(t) = u_T(t) - u_R(t) - 1 = -\sqrt{3}M\cos(\omega t - \theta_0 - \frac{2\pi}{3}) - 1 \end{cases}$$

Section 6
$$\begin{cases} u_R'(t) = u_R(t) - u_T(t) + 1 = \sqrt{3}M\cos(\omega t - \theta_0 - \frac{2\pi}{3}) + 1 \\ u_S'(t) = u_S(t) - u_T(t) + 1 = -\sqrt{3}M\cos(\omega t - \theta_0) + 1 \\ u_T'(t) = +1 \end{cases}$$
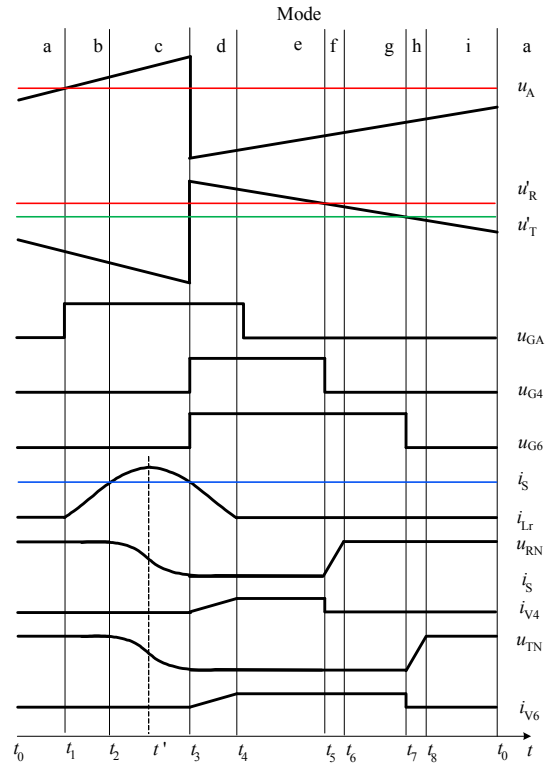(2)

Fig. 3. Waveforms of the ARCP circuit.

From the above analysis, by comparing the modulation wave to the saw-tooth carrier, the gate drive signals $u_{G1} \sim u_{G6}$ are obtained for each power switch in all of the bridges. This is shown in Fig. 2.

III. RESONANCE MODE

In Fig. 2, when one phase current is negative while the other two are positive, the power switch V_A is working and resonance happens. Conversely, if one phase current is positive while the other two are negative, V_B is working. Since the respective phases' currents are direct opposite, the ARCP circuit also has two operation modes, one of which is described in detail below.

Take section 1 as an example, when the three phase current directs as $i_S > 0$, $i_R > 0$, and $i_T < 0$, the power switches V_2 and V_5 in the T phase bridge are off, V_1 and V_2 in the R and S phases upper bridge are off, while V_4 and V_6 in the lower bridge and the auxiliary switch V_A are on.

Fig. 3 shows the waveforms of the ARCP circuit. In per cycle of the carrier, 9 modes can be separated by the main circuit switching manners, which are shown in Fig. 4. Since the frequency of the rectifier carrier is much higher than the grid frequency, the input current in per cycle can be considered constant, and is represented by the constant current source i_s. Meanwhile, since the split-capacitors C_{d1} and C_{d2} are large enough, their voltages are considered constant, and it represented by the voltage source $E_d/2$.
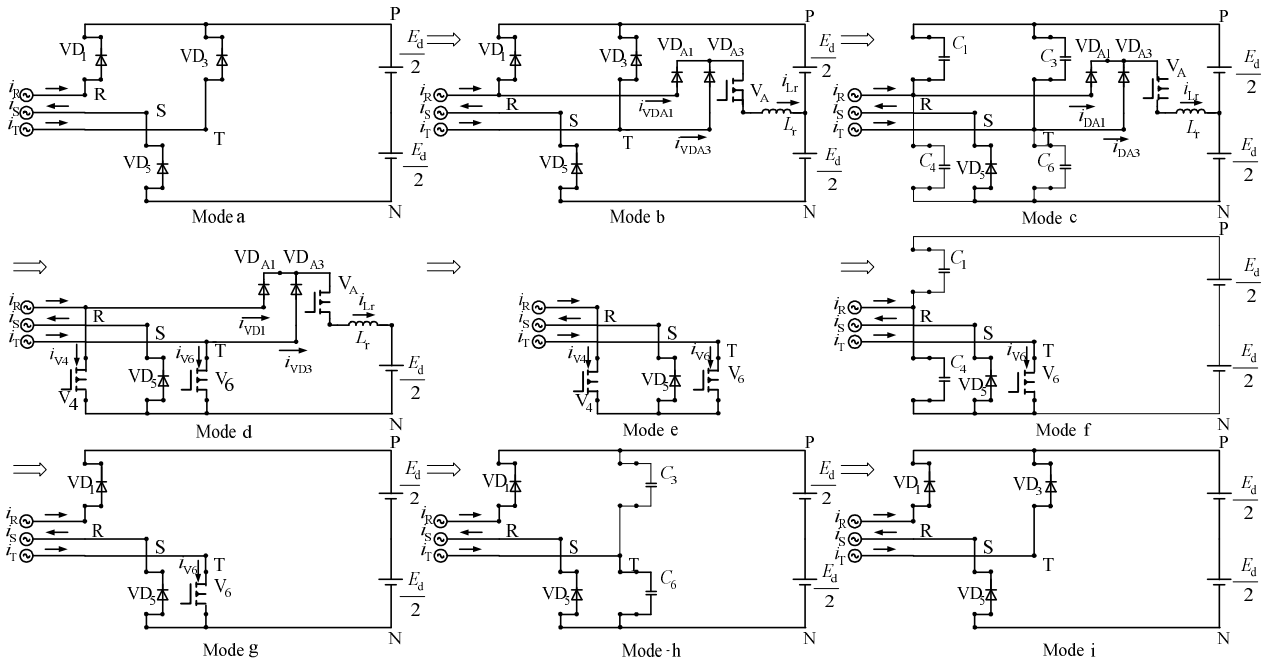
Fig. 4. Operating modes.

A. Resonance Analysis

Mode a ($t_0 \sim t_1$): At the stable state, power is provided to the load from the three phase source and series inductors L_R, L_S and L_T. Each phase current flows through the fly-wheel diodes VD_2, VD_3 and VD_5 respectively.

Mode b ($t_1 \sim t_2$): When V_A switches on at t_2, the voltage on L_r is $E_d/2$, and the current i_{Lr} increases gradually so that V_A is switched on under zero current. When $i_{Lr} = i_{DA1} + i_{DA3} \geq i_R + i_T (= |i_S|)$, diodes VD_1 and VD_3 are shut off at the zero current state.

Mode c ($t_2 \sim t_3$): Resonance happens on both L_r and the snubber capacitors of R and T phases. For R phase, C_1 is charging and C_4 discharging, while for T phase, C_3 is charging and C_6 discharging. During the weakening of the discharge, i_{Lr} increases and then decreases until the discharging of C_4 and C_6 finish at a time when the phase voltage equals zero.

Mode d ($t_3 \sim t_4$): At $t=t_3$, u_{RN} and u_{TN} decrease to zero, and $i_{Lr} = |i_S|$. Therefore, V_4 and V_6 are switched on under zero voltage and zero current.

The voltage on the inductor is $E_d/2$. Therefore, the power directs to source $E_d/2$ and i_{Lr} decreases. At the same time, as i_{V4} and i_{V6} increase, power is transmitted to the series inductors L_R, L_S and L_T. As a result, the current meets with the relations below:

$$|i_S| = i_R + i_T = (i_{V4} + i_{DA1}) + (i_{V4} + i_{DA3}) = (i_{V4} + i_{V4}) + i_{Lr} \quad (3)$$

Since i_S remains constant, $i_{Lr} = 0$ when $|i_S| = i_R + i_T = i_{V4} + i_{V6}$.

Mode e ($t_4 \sim t_5$): i_{Lr} continues to decrease until its direction is reversed. Since diode VD_{A1} and VD_{A3} are off in reverse, the current on i_{Lr} remains zero. As a result, V_A is switched off under zero current.

Mode f ($t_5 \sim t_6$): Since the voltage on capacitor C_4 is zero and is kept there, V_4 can be switched off under zero-voltage. At this time i_{V4} decreases to zero, C_4 starts charging and C_1 starts discharging.

Mode g ($t_6 \sim t_7$): At t_6, u_{RN} increases to E_d, and the voltage on C_1 is zero. At this time, power is transmitted to the load form the R and S phase sources and the series inductors L_R and L_S. As a result, diode VD_1 is switched on by the forward voltage.

Mode h ($t_7 \sim t_8$): Similar to mode f, V_6 is switched off under zero voltage. Meanwhile, i_{V6} decrease to zero, C_6 start charging and C_3 starts discharging.

Mode i ($t_8 \sim t_0$): Similar to mode g, diode VD_3 is switched on. At this time, operation returns to mode a.

B. Mathematical Analysis of the Resonance

1) Mathematical Analysis for Mode b: Due to the initial conditions $i_{Lr}(t_1) = 0$ and $u_{Lr} = E_d/2$, the voltage complies with:

$$L_r \frac{di_{Lr}}{dt} = \frac{E_d}{2} \quad (4)$$

and it can be derived that:

$$i_{Lr}(t) = \frac{E_d}{2L_r}(t - t_1) \quad (5)$$

at $t=t_2$, $i_{Lr}(t_2) = |i_S|$, i.e.

$$i_{Lr}(t_2) = \frac{E_d}{2L_r}(t_2 - t_1) = |i_S| \quad (6)$$
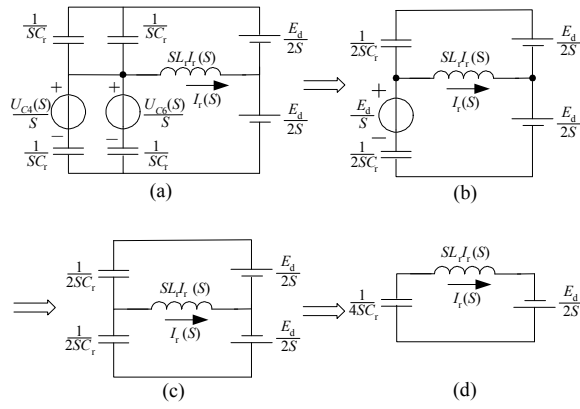
Thus:

Fig. 5. Diagrams of simple equivalent resonant circuit.

$$\Delta t_2 = t_2 - t_1 = \frac{2L_r |i_S|}{E_d} \quad (7)$$

2) Mathematical Analysis for Mode c: Fig. 5 shows diagrams of a simple equivalent resonant circuit. Assume that each capacitor is C_r, and that the initial conditions are $u_{C4}(t_2)=u_{C6}(t_2)=E_d$, i.e. $U_{C4}(S)= U_{C6}(S)=E_d/S$. Then the resonant current $i_r(t_2)=0$. For Fig. 5d, the following equation can be satisfied:

$$\frac{1}{4SC_r} I_r(S) + SL_r I_r(S) = \frac{E_d}{2S} \quad (8)$$

The solution gives:

$$I_r(S) = E_d \sqrt{\frac{C_r}{L_r}} \frac{\omega_r}{S^2 + \omega^2_r} \quad (9)$$

Where: $\omega^2_r = \dfrac{1}{4L_r C_r}$

So that:

$$i_r(t-t_2) = E_d \sqrt{\frac{C_r}{L_r}} \sin \omega_r(t-t_2) \quad (10)$$

at $t=t'$, i.e. when i_r comes to its maximum, and makes a derivative with both parts of Equation (10). Moreover, let the left part be:

$$\frac{di_r(t-t_2)}{d(t-t_2)}=0 , \quad \text{then: } \cos\omega_r(t_1-t_2)=0$$

It can be obtained that:

$$\Delta t' = t - t_2 = \frac{\pi}{2\omega_r} = \pi\sqrt{L_r C_r} \quad (11)$$

In Fig. 5a, the voltage on capacitors C_4 and C_6 are:

$$U_{C4}(S) = U_{C6}(S) = \frac{E_d}{S} - SL_r I_r(S) - \frac{E_d}{2S} \quad (12)$$

Substitute (8) into the above equation, then:

$$U_{C4}(S) = U_{C6}(S) = \frac{E_d}{2S} - \frac{E_d}{2} \cdot \frac{S}{S^2 + \omega_r^2} \quad (13)$$

The solutions show that:

$$u_{c4}(t-t_2) = u_{c6}(t-t_2) = \frac{E_d}{2}[1-\cos\omega_r(t-t_2)] \quad (14)$$

By substituting (11) into (14), it can be seen that the voltages on C_4 and C_6 comply with (15) when i_r comes to its maximum:

$$u_{C4}(\Delta t') = u_{C6}(\Delta t') = \frac{E_d}{2} \quad (15)$$

When C_4 and C_6 discharge at $t=t_3$, their voltages become zero. Therefore, let (14) equals zero, which results in:

$$\cos\omega_r(t_3-t_2)=1$$

$$\Delta t_3 = t_3 - t_2 = \frac{\pi}{\omega_r} = 2\pi\sqrt{L_r C_r} \quad (16)$$

Integrating (16) and (10), i.e. at $t=t_3$, the resonant current i_r follows:

$$i_r(\Delta t_3)=i_r(t_3-t_2)=0 \quad (17)$$

It can be seen that, when i_{Lr} reaches its maximum, the voltages on C_4 and C_6 decrease from E_d to $E_d/2$. This is due to the fact that when $u_{C4}(u_{C6})>E_d/2$, the voltage on L_r is positive ($u_{C4}-E_d/2>0$). Therefore, as i_{Lr} increases (for $i_{Lr}=i_{Lr}(t_2)+i_r(t-t_2)=i_S+i_r(t-t_2)$), power accumulates gradually on L_r. Moreover, when $u_{C4}(u_{C6})=E_d/2$, the voltage added on L_r becomes zero. Then i_{Lr} stops increasing, i.e. i_{Lr} comes to its maximum. As C_4 and C_6 discharge, $u_{C4}(u_{C6})$ start to decrease until $u_{C4}(u_{C6})<E_d/2$. Therefore, the voltage on L_r turns to be negative. Then due to the converse $L_r di_{Lr}/dt$, i_{Lr} starts to decrease and release energy from L_r, which equals the accumulated energy as mentioned above. Finally, at $t=t_3$, $i_{Lr}=i_{Lr}(t_2)+i_r(t-t_2)=i_S$.

3) Working time of the auxiliary switch V_A: For the sake of convenience, Fig. 3 use a saw-tooth carrier with a positive slope for a comparison of the voltages. The time when V_A is switched on or when resonance starts is determined by u_A. As shown in Fig. 3, the time that V_A closes is ahead of the vertical edges of the saw-tooth carrier, namely at t_1. According to the above analyzes in 1) and 2), the advance time shall be $(\Delta t_2+\Delta t_3)$.

Assume that the carrier period is T_c, the reference voltage u_A can then be derived from:

$$\frac{u_A+1}{2} = \frac{T_c - (\Delta t_2 + \Delta t_3)}{T_c} \quad (18)$$

Or: $$u_A = 1 - \frac{2(\Delta t_2 + \Delta t_3)}{T_c}$$

Substituting (7) and (16) into this yields:

$$u_A = XI + Y \quad (19)$$

Where: $X=\dfrac{4L_r}{T_c E_d}$ and $Y=1-\dfrac{4\pi\sqrt{L_r C_r}}{T_c}$, $I=|i_S|$

From Equation (19), the time that V_A switches on should vary with changes in i_S. In other words, it can follow the fluctuation of the load. However, the time when V_A switches off should be behind of the vertical edges of the saw-tooth carrier, and its delay time should be longer than $(t_4-t_3\approx\Delta t_3)$.

A positive slope saw-tooth carrier can also be used to get solutions for the reference voltages u_A or u_B in all of the sections shown in Fig. 2. Equation (19) is also adaptable to all of the sections except that the reference current I should be valued as bellow:

Section 1 and 4, $I=|i_S|$
Section 2 and 5, $I=|i_R|$
Section 3 and 6, $I=|i_T|$

As above mentioned, when V_A works, the resonance makes the input voltage of the bridges periodically decrease to zero, which provides the ZVS condition for the switches in the lower bridges. On the other hand, when V_B works, the resonance will periodically increase the input voltage of the bridges to E_d, which creates ZVS for the switches in the upper bridges.

4) Design of the Resonance Parameters: The selection of resonance parameters considers not only achievement of zero-voltage soft-switching, but also the resonance time, the current and voltage stress, and additional losses, etc.

From (10) and (11), the maximum value for i_r can be deduced as follows:

$$I_{rmax} = E_d\sqrt{\frac{C_r}{L_r}} = \frac{E_d}{Z_r} \qquad (20)$$

Where, the resonance impedance $Z_r = \sqrt{\frac{L_r}{C_r}}$.

The resonant current i_r affects the current stress, the on-state losses, and the turn-off losses of the auxiliary switches. Since the DC voltage E_d is related to the modulation ratio M, according to (20), the adjustable parameter affecting the resonant current is Z_r.

From the viewpoint of reducing loss, it is hoped that the resonant current is as small as possible, i.e. Z_r is as large as possible. This can be achieved by increasing C_r or by reducing L_r. However, too much Z_r can also cause problems.

The resonant capacitor C_r should be optimized to ease the main switch turn-off loss in case it is too small [18].

Since L_r is related to the load current, too large a value for L_r might cause a prolonged rise time for i_r, and it might affect the normal resonance.

Therefore, the determination of Z_r should meet with the resonance time at first, and consider the circuit loss [19].

The maximum commutation time $(\Delta t_2+\Delta t_3)$ should be smaller than the switching dead time t_{dead} of traditional hard-switching inverters, i.e. $\Delta t_2+\Delta t_3 < t_{dead}$. According to Equations (7) and (16), $(\Delta t_2+\Delta t_3)$ can be expressed as:

$$\frac{2L_r I_{Smax}}{E_d} + 2\pi\sqrt{L_r C_r} \le \Delta t_2 + \Delta t_3 < t_{dead} \qquad (21)$$

Where, I_{Smax} is the maximum for i_s.

The resonant frequency ω_r should be set by optimizing the current stress, the on-state losses and the turn-off losses of the auxiliary switches.

With the load current I_{Smax}, the resonance current I_{rmax}, and the optimized resonant capacitor C_r, the resonant inductance L_r is decided.
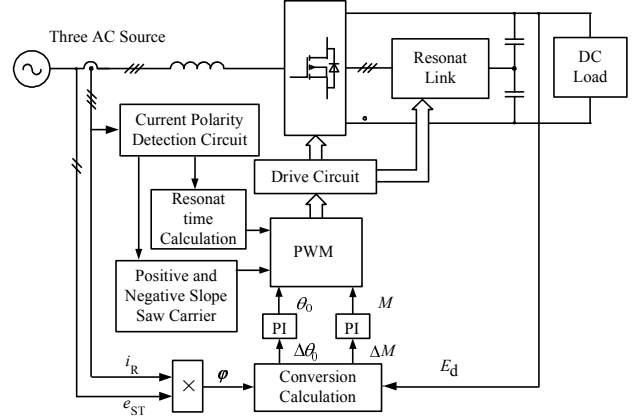

Fig. 6. Block diagram of control system.

IV. SIMULATION AND EXPERIMENTAL RESULT

A. Control System

The control system shown in Fig. 6 includes two parts:

One part aims at realizing power factor correction (PFC) and keeping the DC-bus voltage constant. By measuring the line voltage e_{ST} and phase current i_R, the power factor angle φ can be obtained after phase discrimination. Then it is transformed as the angle offset $\Delta\alpha$, which is used in the PI regulator for phase control. By probing the DC bus voltage E_d, the value is transformed into the modulation ratio offset ΔM, which is used in the PI regulator for voltage control. The two PI regulators are realized by the following software algorithm:

$$\theta_0(n+1) = \theta_0(n) + (k\Delta\theta_0 + \int\Delta\theta_0 dt) \qquad (22)$$

$$M(n+1) = M(n) + (k\Delta M + \int\Delta M dt) \qquad (23)$$

Based on the phase and amplitude control method, the three-phase modulation waves can be derived from Equation (2).

The other part is to ensure that the ARCP circuit works in the soft-switching state. By detecting the direction of the three-phase current, the saw-tooth carrier adopts a positive slope or a negative slope. Then it compares this with the modulation waves and the PWM drive signals can be produced. By measuring the amplitude of the phase current, the auxiliary switch drive signals can be obtained according to Equation (13).

B. Current Feedback Control

Fig. 7 shows the phasor adjusting method for the rectifying mode, where the lag angle θ_0 is the angle between phasors $\dot{E}_R$ and $\dot{U}_R$. U_R is the virtual value of the fundamental component of phase R produced by PWM. It is deduced as:
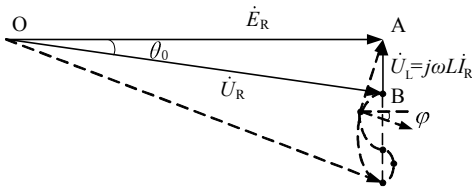
Fig. 7. The Phasor adjusting method for rectifying mode.

$$U_R = \frac{ME_d}{\sqrt{3}\sqrt{2}} = \frac{ME_d}{\sqrt{6}} \tag{24}$$

For improving the system dynamic response, the transition curve near the upright side of the triangle in Fig. 8 should be shortened. In Fig. 8 on the condition of ensuring a unity power factor and a constant DC-bus voltage, when there is a sudden load increase, the converter cannot offer a sudden current immediately to series inductance in input side of the converter, at the time only capacitors can offer the sudden current, thus the output DC current of the system next steady state is expressed by

$$I^*_d = I_d + I_c = I_d + C\frac{du_c}{dt} \tag{25}$$

By following the energy balance between the AC side and the DC side of the converter, the following is obtained:

$$3E_R I^*_R = E_d I^*_d = E_d(I_d + c\frac{du_c}{dt}) \tag{26}$$

For u_c is E_d, with the right angle triangular diagram, (26) can be rewritten as:

$$\tan(\theta_0 + \Delta\theta_0') - \tan\theta_0 = \frac{\omega L E_d}{3E_R^2}C\frac{dE_d}{dt} \tag{27}$$

Taking $\Delta\theta_0'$ as small, (27) is linearized as:

$$\Delta\theta_0' \approx k_1\frac{dE_d}{dt} \tag{28}$$

where: $k_1 = k_0\dfrac{\omega LCE_d}{3E_R^2}$, $k_0 \approx \dfrac{\Delta\theta_0'}{\tan(\theta_0 + \Delta\theta_0') - \tan\theta_0}$

In a way similar to the $\Delta\theta_0'$ derivation, according to the right-angled triangle relations between phasors, the following is obtained:

$$I^*_R = \frac{(M + \Delta M')E_d}{\sqrt{6}\omega L}\sin(\theta_0 + \Delta\theta_0') \tag{29}$$

The change of the modulation is deduced as:

$$\Delta M' \approx -\frac{k_2 M\Delta\theta_0'}{\sin(\theta_0 + \Delta\theta_0')} + \frac{k_3}{\sin(\theta_0 + \Delta\theta_0')}\frac{dE_d}{dt} \tag{30}$$

where, k_2 and k_3 are the proportion factor.
When the second portion in (30) is small and can be omitted, (30) approximates to:

$$\Delta M' \approx -\frac{k_2 M\Delta\theta_0'}{\sin(\theta_0 + \Delta\theta_0')} \tag{31}$$

From (28) and (31), it is known that the variable load current is detected indirectly by a change of the DC voltage. This feeds the control system for the next steady state as an additional control variable to generate $\Delta\theta_0'$ and $\Delta M'$. Therefore, the system control equation is:
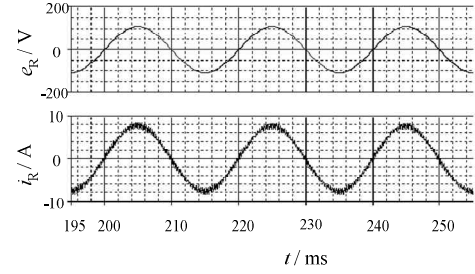
(a) Waves of voltage and current for Phase R.
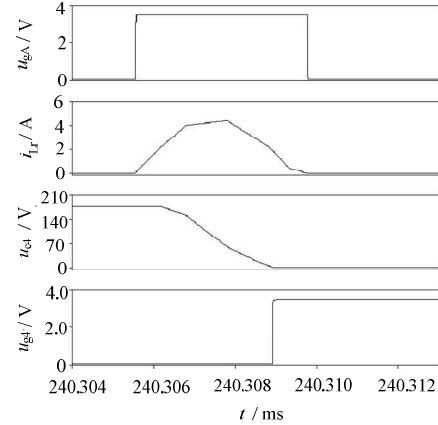
(b) Resonance waves.

Fig. 8. Simulation waveforms.

$$\theta_0(n+1) = \theta_0(n) + (k\Delta\theta_0 + \int\Delta\theta_0 dt) + \Delta\theta_0' \tag{32}$$

$$M(n+1) = M(n) + (k\Delta M + \int\Delta M dt) + \Delta M' \tag{33}$$

C. Simulation Verification

Accordingly the control system in Fig. 6, a simulation model based on Pspice software is built. The main parameters used in the simulation are as follows:

Input line voltage: 110V
DC voltage: 190V
Inductors: $L_{R, S, T}$ =7mH
Split-capacitors: C_{d1}= C_{d2}=1100μF
Snubber capacitors: C_{1-6}=8nF
Resonant inductor: L_r=14μH
Carrier frequency: f_c=3.3kHz

Fig. 8 shows the simulation waveforms. In Fig. 8(a) the upper curve is the R phase voltage e_R, and the lower curve is the R phase current i_R. In Fig. 8(b), from top to bottom, the curves are the voltage u_{gA} of the V_A driver signal, the voltage u_{c4} of snubber C_4, the current i_{Lr} of the inductor L_r, and the voltage u_{g4} of the V_4 driver signal.
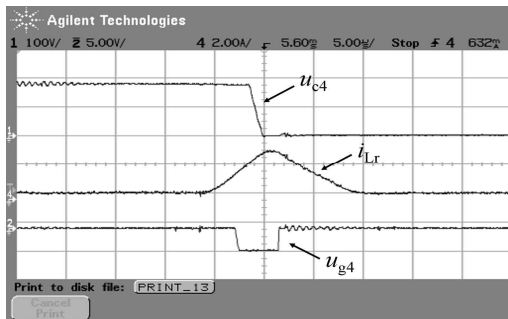
In Fig. 8, the input phase R current keeps in phase with the source phase R voltage. In the process of the system power conversion, the main switch turns on under the ZVS condition, and the auxiliary switch conducts in the ZCS state. The simulation results conform to the theory discussed previously.
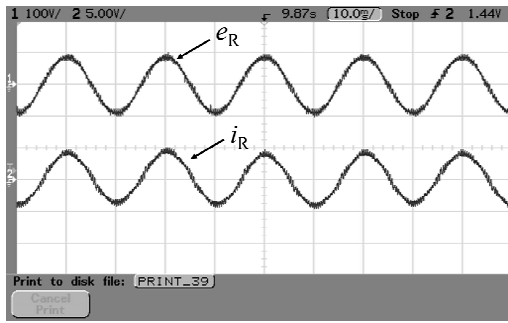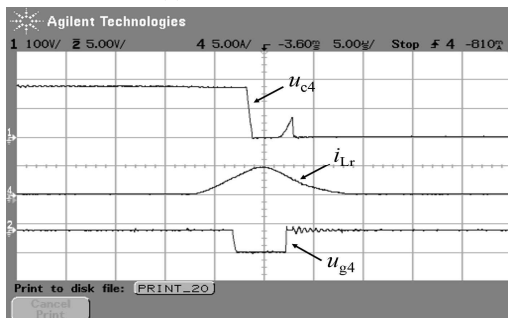
(a) Waves of voltage and current for Phase R.
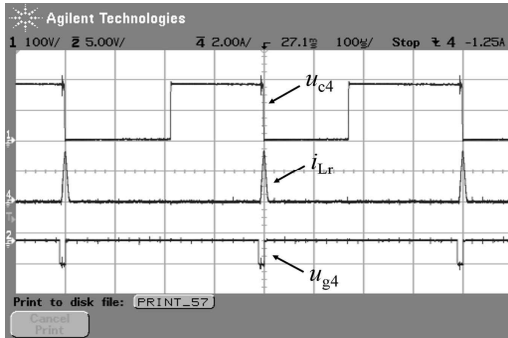
(b) Resonance on ZVS.

(c) Resonance on ZVS.

(d) Resonance not on ZVS.

Fig. 9 Experimental waveforms.

D. Experimental Results

A 1kW prototype system is constructed for experimental verification. The system control is implemented on a platform consisting of a digital signal processor (DSP). The main parameters used in the experiment are as same as those used in the simulation.
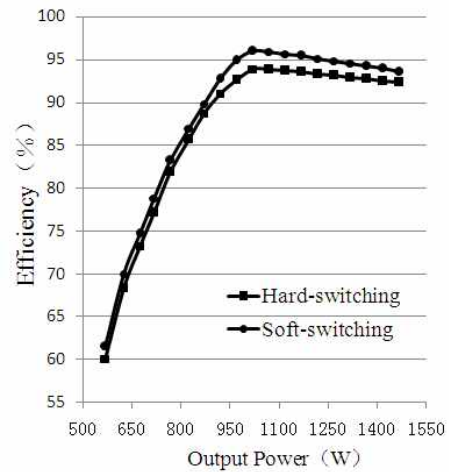

Fig. 10. Efficiency Comparison.

The experimental results obtained from the prototype system are shown in Fig. 9.

Fig. 9(a) shows in rectifying state, where the total input power factor (PF) of the phase current is 99.85% and the total harmonic distortion (THD) is 5.4%.

Fig. 9(b)-9(d) show the experimental waveforms for the resonance of the ZVS. Fig. 9(c) is a partially enlarged detail drawing of Fig. 9(b). As can be seen, when u_{c4} is discharged to zero for resonance, the turning-on of V_4 is in the zero voltage state.

Because the voltage of the snubber capacitor cannot change immediately, the power switches always turn off in zero voltage.

If the turning-on time of G_{v4} is delayed 1μs, the voltage u_{c4} will rise owing to the energy of the resonant inductor, and the turning-on of V_4 is not in the zero voltage state.

Fig. 10 shows the converter efficiency versus the output power. The efficiency of the soft-switching rectifier improves by about 2.1% at 1.02kW when compared with the conventional SPWM hard-switching topology.

V. CONCLUSIONS

An auxiliary resonant commutated pole topology for three-phase PWM rectifiers is proposed. A detailed analysis and experiments are given based on its working principle, control strategy and resonant modes. Simulation and experiment results prove the consistency on a mathematical basis.

The proposed rectifier shows improvements on simpler structures when compared to the conventional ARCP while maintaining its efficiency. As a result, it is achieves cost-savings in hardware due to its simplified main circuit topology. Nonetheless, the minimum peak current in resonating and the least switching PWM mode enhance its advantages of high efficiency and easy control.

REFERENCES

[1] S. Sato, Y. Suehiro, S. I. Nagai, and K. Morit, "High efficiency soft-switching 3-phase PWM rectifier," in *Proc. INTELEC*, pp. 453-460, Sep. 2000.

[2] J. Yoshitsugu, K. Inoue, E. Hiraki, and M. Nakaoka, "Resonant DC link snubber-assisted soft switching inverter type AC servo driver with low common mode current characteristics," in *Proc. IEEE Conf. Power Electron. Drive Syst.*, pp.494-499, Oct. 2001.

[3] T. Ahmed, S. Nagai, M. Nakaoka, and T. Tanaka, "Utility-interactive four-switch three-phase soft-switching inverter with single resonant DC-link snubber and boost chopper," *Journal of Power Electronics,* Vol. 7, No. 2, pp.109-117, Apr. 2007.

[4] K. Q. Qu, C. B. Sun, G. C. Chen, C.Y. Xu, and T. Katsunori, "A PAC based three-phase zero-voltage soft-switching PWM converter," in *Proc. IEEE the 4th IPEMC*, Vol. 3, pp. 1091-1096, Aug. 2004..

[5] L. Rui, and D. H. Xu, "A Zero-Voltage Switching Three-Phase Inverter," *IEEE Trans. Ind. Electron.*, Vol. 29, No. 3, pp.1200-1210, Mar. 2014.

[6] R. W. De Doncker and J. P. Lyons, "The auxiliary resonant commutated pole converter," in *IEEE IAS Conf. Rec.*, pp. 1228-1235, Oct. 1990.

[7] E. Chu, M. Wu, L. Huang, X. Hou, and H. Zhang, "Research on a novel modulation strategy for auxiliary resonant commutated pole inverter with the smallest loss in auxiliary commutation circuits," *IEEE Trans. Power Electron.*, Vol. 28, No. 3, pp. 1103-1117, Mar. 2013.

[8] Z. Y. Ma, D. H. Xu, R. Li, C. R. Du, and X. Zhang, "A novel dc-side zero-voltage switching (ZVS) three-phase boost PWM rectifier controlled by an improved SVM method," *IEEE Trans. Power Electron.*, Vol. 27, No. 11, pp. 4391-4408, Nov. 2012.

[9] Q. Zhang, H. Hu, D. Zhang, X. Fang, Z. Shen, and I. Bartarseh, "A controlled-Type ZVS technique Without Auxiliary Components for the low power DC/AC inverter," *IEEE Trans. Power Electron.*, Vol. 28, No. 7, pp. 3287-3296, Jul. 2013.

[10] M. Marvi and F. Ali, "A fully ZVS critical conduction mode boost PFC." Power Electronics," *IEEE Trans. Power Electron.*, Vol. 27, No. 4, pp. 1958-1965, Apr. 2012.

[11] J. Aguillon-Garcia and G.-W. Moon, "A high-efficiency three-phase ZVS PWM converter utilizing a positive double-star active rectifier stage for server power supply," *IEEE Trans. Ind. Electron.*, Vol. 58, No. 8, pp. 3317-3329, Aug. 2011.

[12] R.Corentin, F. Jean-Paul, Le, M. Philippe, D. Philippe, and L. Alain, "A simplified resonant pole for three-level soft-switching PFC rectifier used in UPS," *IEEE Trans. Ind. Electron.*, Vol. 57, No. 8, pp. 2739-2746, Aug. 2010.

[13] W. Dong, J. Y. Choi, F. C. Lee, D. Boroyevich, and J. Lai, "Comprehensive evaluation of auxiliary resonant commutated pole inverter for electric vehicle applications,"

in *Proc. IEEE PESC*, Vol. 2, pp. 625-630, Jun. 2001.

[14] Y. Jang and M. M. Jovanovic, "The TAIPEI rectifier-a new three-phase two-switch ZVS PFC DCM boost rectifier," *IEEE Trans. Ind. Electron.*, Vol. 28, No. 2, pp. 686-694, Aug. 2013.

[15] M. R. Amini, and H. Farzanehfard, "Three-phase soft-switching inverter with minimum components," *IEEE Trans. Ind. Electron.*, Vol. 58, No. 6, pp. 2258-2264, Aug. 2011.

[16] K. Nishimura, K. Hirachi, A. M. Eid, H. W. Lee, and N. Nakaoka, "A novel prototype discontinuous inductor current mode operated three-phase PFC power converter with four active switches," in *Proc. IEEE PESC*, pp. 824–830, Jun. 2006.

[17] Q. Zhang, D. H. Zhang, H. B. Hu, J. Shen, and I. Batarseh, "Controlled-type ZVS technique without auxiliary components for micro-inverters," *Journal of Power Electronics*, Vol. 13, No. 6, pp. 919-927, Nov. 2013

[18] R. L. Steigerwald, R. W. De Doncker, and M. Kheraluwala, "A comparison of high power dc–dc soft switched converter topologies," *IEEE Trans. Ind. Applicat.*, Vol. 32, No. 5, pp. 1139-1145, Sep./Oct. 1996.

[19] E. H. Chu, M. Y. Wu, L. Huang, X. Hou, and H. G. Zhang, "Research on a novel modulation strategy for auxiliary resonant commutated pole inverter with the smallest loss in auxiliary commutation circuits," *IEEE Trans. Power Electron.*, Vol. 29, No. 3, pp. 1103-1117, Mar. 2014.

Ke-Qing Qu was born in China, in 1970. He received his Ph.D. degree in Electrical Engineering from Shanghai University, Shanghai, China, in 2004. He is currently an Associate Professor at the Shanghai University of Electric Power, Shanghai, China. He is also a Master Instructor. As a Visiting Scholar, he studied in Germany with full funding by the National Foundation for Study, from 2009 to 2010. He holds three Chinese patents and one monograph. He has published more than 40 technical papers in journals and conference proceedings. His current research interests include power electronic conversion, and new energy generation and its application to power systems.

Jin-Bin Zhao (M'06) was born in China, in 1972. He received his M.S. and Ph.D. degrees in Electrical Engineering from Oita University, Oita, Japan, in 2002 and 2005, respectively. He worked as a Researcher at the R&D Headquarters of the Origin Electric Co., Ltd, Japan, from 2005 to 2011. He is currently a Professor at the Shanghai University of Electric Power, Shanghai, China. He currently holds three U.S. patents and ten Japanese patents. He has published 60 technical papers in journals and conference proceedings. His current research interests include the control of power converters, soft-switching power converters, inverters, distributed power systems, power-factor correction and electric drive systems. Dr. Zhao is a Member of the Institute of Electrical and Electronics Engineers (IEEE), the Institute of Electrical Engineers of Japan (IEEJ), and the Institute of Electronics Information and Communication Engineers of Japan (IEICE). He is also a Senior Member of the China Power Supply Society.